Journal of Physics: Conference Series

Farm wide sensitivity assessments of resonant frequencies of integrated offshore wind turbine finite element models

To cite this article: D J M Fallais *et al* 2022 *J. Phys.: Conf. Ser.* **2265** 042053

Farm wide sensitivity assessments of resonant frequencies of integrated offshore wind turbine finite element models

D J M Fallais[1], K Winkler[1], C Sastre Jurado[1,2], W Weijtjens[1], B Stuyts[1,2] and C Devriendt[1]

[1] Vrije Universiteit Brussel, OWI-lab, AVRG, Pleinlaan 2, 1050, Brussels, Belgium
[2] UGent, Geotechnical Laboratory, Technologiepark 68, Zwijnaarde, 9052, Belgium

E-mail: `dominik.fallais@vub.be`

Abstract. To date, despite advancements in the design of offshore wind turbines, the as-designed and identified as-built natural frequencies of offshore wind turbines still show discrepancies. These discrepancies are partially rooted in modelling uncertainties, as well as uncertain input parameters, related to e.g. aero-, fluid- or soil-structure interaction. The first objective of this article is to present a wind farm wide comparison of the first and second, modelled and identified, fore-aft natural frequencies for turbines in parked conditions for a wind farm located in the Belgian north sea. Secondly, the effect of different model parameters on the computed natural frequencies will be assessed using wind farm wide sensitivity studies, with the aim to describe the potential of each considered parametrization in reducing the discrepancy between modelled and measured resonance frequencies. The in-depth considered parametrizations are aimed at assessing the effect of the linearization of the p-y curves, soil stiffness, local scour as well as the mass of the rotor nacelle assembly, whereas results for wall thickness, marine growth, added mass coefficient and sea water level variations will be presented without further discussion. In order to perform this study, turbine specific finite element models have been prepared and verified based on detailed design documents; subsequently updated best-estimate soil data has been used to model the foundation for two different design scenarios. Furthermore, modal parameters have been identified for each turbine, based on vibration data collected in parked condition and state of the art operational modal analysis tools. The results show that the discrepancies between the modelled and identified first fore-aft natural frequencies could potentially be bridged by adjusting combination of the investigated parameters, whereas the discrepancies observed on the second natural frequency cannot be bridged by making changes to the investigated parameters. As such, future work will entail a more detailed investigation on modelling uncertainties.

1. Introduction

During the past years the On- and Offshore Wind Infrastructure Application Lab (OWI-Lab), in collaboration with industry partners, has conducted a large number of design verification campaigns, allowing to identify the resonance frequencies of offshore wind turbines using vibration measurements at parked conditions [8]. Despite advancements in the design of offshore wind turbines, the modal properties of as-designed offshore wind turbines do still show discrepancies with respect to the identified (as-built) modal properties [14, 16, 20, 18]. Parts of these discrepancies are rooted in uncertain input parameters, as well as modelling uncertainties related to e.g. soil or fluid-structure interaction. On the other hand, time varying environmental conditions, such as scour or tidal levels, affect the measured as-built natural frequencies as well.

Reducing the observed differences between as-designed modal properties and the measured modal properties over the full range of the operational and environmental conditions is essential for several fatigue monitoring applications. These applications often rely on accurate finite element models in order to extrapolate operational strain measurements at easily accessible locations to arbitrary unmeasured locations [12, 15]; furthermore lower modelling uncertainties potentially can result in more efficient future designs. Hence, model updating and uncertainty quantification can be relevant for built infrastructure as well as future developments. For that purpose, deterministic and stochastic model updating techniques can be used, with the goal to tune parameters of numerical models, such that e.g. the modal parameters of the considered numerical model correspond to modal parameters identified from vibration measurement data [19, 3, 17]. This article presents intermediate steps towards farm wide model updating based on identified natural frequency data, as well as an integrated finite element model.

The first objective of this contribution is to compare the differences between measured and modelled natural frequencies during parked conditions. As part of this comparison, the difference between the as-designed and best estimate in-house model will be described in Section 2. Subsequently, the identified and as-designed natural frequencies are presented in Section 3 as the percentage deviation with respect to the frequencies computed with the nominal in-house model. The second objective is aimed at the goal of performing fleet-wide turbine specific model updating; for that purpose four sensitivity studies will be conducted, each describing the effectiveness of a specific parametrization in reducing the discrepancies between the measured and observed first and second order natural frequencies. Turbine specific model sensitivities with regard to the linearization of the p-y curves, soil stiffness, local scour, and the mass of the rotor nacelle assembly, are presented and discussed in Section 4. Whereas Appendix A presents tabulated sample statistics for the model sensitivities due to wall thickness, marine growth, added mass coefficient and sea water level variations. All presented sensitivities are expressed in terms of the percentage change of the first and second fore-aft natural frequency with respect to the frequencies computed with the nominal in-house model.

Results indicate that the measured natural frequencies are considerably higher than the as-designed frequencies. Using the in-house model with the initial soil stiffness as basis for deriving soil spring coefficients, bridges the discrepancies on the first order frequencies to a degree which could be explained by the effect of several parameters. However the observed discrepancies on the second order frequencies could not be reduced sufficiently, and motivate a deeper investigation of modelling uncertainties, especially with regard to higher order modes.

2. Data and model description

This section will briefly describe the identified natural frequency data, the as-designed frequencies, as well as the integrated finite element model which has been used to compute natural frequencies. Furthermore an overview of the parametrizations used for the sensitivity assessments will be given.

2.1. Design verification data

Extensive design verification campaigns have been conducted on a farm-wide level during parked operating conditions. Each campaign has resulted in high frequency acceleration data, which was recorded by a mobile measurement unit containing a multi-axial accelerometer (Figure 1), and processed into natural frequency estimates by state of the art system identification methods [10, 9]. In order to account for varying tidal levels during individual measurement runs, the second fore-aft and side-side frequency have been corrected using a linear correction of -0.0205 Hz/m which was determined using measurement data from turbines which have a permanent monitoring system. The Tidal data needed for this correction has been obtained from the nearest public met-ocean station; this data is provided to the public by the Belgian Agency for Maritime and Coastal Services [1].

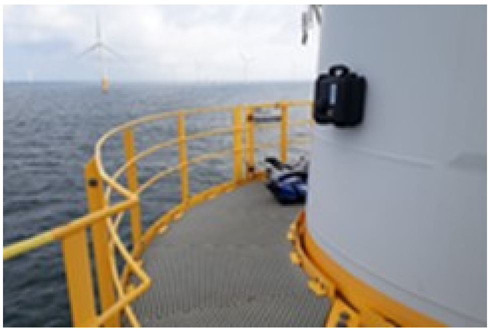

Figure 1. Mobile measurement system containing accelerometers.

2.2. As-designed data

Detailed design documentation and as-designed frequencies are available for several design scenarios. For this contribution two design scenario's are considered: the "Nominal" design scenario, which is used for the fatigue design and should result in representative average natural frequencies for an operational turbine throughout its design lifetime; the "Stiff" design scenario, which assumes the initial soil stiffness, maximum soil accretion, no corrosion allowance, no marine growth as well as extreme low water levels. The combined effect of the latter assumptions results in the upper bound of the as-designed natural frequencies. For the nominal design scenario the designer assumed a representative load case in order to obtain linearized lateral soil spring stiffness values; the derived spring stiffness values are lower than the spring stiffness values based on the initial soil stiffness profile, which is assumed for the stiff scenario. It can be argued that the stiff scenario does loosely correspond to parked conditions, since the initial soil stiffness is the result of linearizing the p-y curves at very small deflection values, which could be more in line with lateral deflection levels of the monopile during parked/idling conditions than operational conditions. The latter observation motivates to consider the stiff case, since all design verification campaigns are conducted in parked condition. An overview of selected modelling assumptions for the as-designed scenarios is presented in Table 1.

Table 1. Overview of used models and modelling aspects

Model aspect	OWI-lab$^{(1)}$	Design: Nominal	Design: Stiff
Scour	no	no	no
Accretion$^{(2)}$	no	no	maximum
Corrosion	no	half of the allowed	no
Marine growth	full	full	no
Soil curves	fatigue design (PISA)	fatigue design	upper bound stiffness
p-y Linearization	representative load	load based on fatigue loads	initial soil stiffness
Water level	mLAT +2m	fatigue weighted average	50 year extreme low
Description	Section 2.3	Section 2.2	

$^{(1)}$ OWI-lab: Nominal, OWI-lab: Nominal-IS
$^{(2)}$ Formation of soil deposits on top of the unscoured mud-line

2.3. Integrated FE model

The support structure is modelled using 1-D Timoschenko beam elements in conjunction with a lumped mass formulation. The rotor nacelle assembly is connected to the tower top by rigid links, and is modelled by point massess as well as rotational inertia terms, both obtained from detailed design documentaion. The monopile foundation is modelled as a linear elastic foundation, i.e. the soil is idealized as a series of independent lateral springs (p-y model), whose stiffness is derived from PISA curves [5, 6]. This choice, instead of using the full PISA formulation [5, 6], is motivated by the relative slender nature of the considered OWT's (L/D: $5.5-7.1$) [11]. Furthermore, a Young's modulus of 210GPa and a Poisson's ratio of 0.3 have been used as default material properties for steel; the weight of the grout connection is accounted for by adding lumped masses, whereas any potential stiffness related to the grout connection is neglected; flanges and secondary steel have been added conform to the technical documentation of the specific OWT's; marine growth is added with a maximum thickness of 150mm and a density of around 1.4 t/m^3 [2]; contained and added water mass are derived using an added mass coefficient of C_m=1.2 [7], and are modelled as lumped masses which are distributed along the water depth. The integrated finite element model is developed in Openseespy [22] and all input data required to setup turbine specific models is managed through the OWI-lab meta-database [4].

For verification purposes the nominal in-house model has been been setup such that it reflects the modelling assumptions made by the designer, which allows to perform a direct verification of the nominal design scenario. In order to replicate the designers models as accurate as possible the p-y curves contained in the design documentation are used. Comparing the computed natural frequencies with the frequencies listed in the design reports, shows that accuracy levels below two percent are realised on the first two fore-aft and side-side frequencies. Subsequent to the verification, the in-house nominal model has been updated with best estimate soil curves, which are based on re-interpreted CPT data in combination with the PISA formulation, as outlined in the previous paragraph.

Next to the nominal scenario, an additional scenario is considered for the comparison presented in Section 3; this scenario is equivalent to the described nominal scenario, but with a maximum stiff foundation (Initial stiffness). The latter scenario should generate frequencies which are more in line with frequencies observed during parked conditions - following the rationale presented in Section 2.2. An overview of selected modelling assumptions for the in-house model as well as the designer's model are presented in Table 1.

Table 2. Model parametrizations and parameter ranges used for sensitivity assessments.

Parametrization	Range	Section
Thrust load for the linearization of the p-y curves	1 [N] - 500 [kN]	4.1
Scaling: spring stiffness values	0.5 - 10 [–]	4.2
Local scour depth	0 - 10 [m]	4.3
Scaling: rotor nacelle assembly inertia terms	0.8 - 1.2 [–]	4.4
Added mass coefficient	1, 2 [–]	Appendix A
Wall thickness	-1, 1 [mm]	
Scaling: marine growth density	0.8, 1.2 [–]	
Sea water level	-1, 2, 5 [mLAT]	

2.4. Overview of model parametrizations
The parametrizations which have been used for the individual sensitivity studies are presented in Table 2. The results of these studies are presented in Section 4 as well as in Appendix A. All parametrizations are symmetric w.r.t. to the fore-aft and side-side direction, therefore the results of the sensitivity studies will only be displayed for the fore-aft direction; a table of sensitivities including results for the side-side direction is presented in Appendix A. The nominal in-house model will be used as base-line model for the sensitivity studies presented in Section 4; furthermore, the natural frequencies computed with this model will be used used as reference throughout the remainder of this work.

3. Natural frequency comparisons
The comparison of the identified, as-designed and computed natural frequencies is presented in Figure 2. For each order, the fore-aft and side-side frequencies have been expressed as percentage change with respect to the frequencies computed with the nominal OWI-lab integrated model (*OWI-Lab: Nominal*). All four sets of farm-wide frequency data have been sorted such that the error between the measured first fore-aft frequency and the corresponding frequencies computed with the *OWI-Lab: Nominal* model are in ascending order.

Figure 2. Comparison of measured frequencies, as-designed frequencies and frequencies computed with the integrated OWI-lab FE model. All frequencies are expressed relative to the corresponding nominal frequencies computed with the *OWI-lab: Nominal* model, and have been sorted such that the error between the measured first fore-aft frequency and the corresponding nominal frequencies are in ascending order. Upper half: first order fore-aft and side-side frequencies. Lower half: second order fore-aft and side-side frequencies.

When comparing the measurement data with the computed natural frequencies in Figure

2, the most obvious finding is that the built OWT structures have higher natural frequencies than their as-designed and computed counterparts. This leads to the general conclusion that the models are not stiff enough, or that masses are severely overestimated. Matching the first order (fore-aft and side-side) frequencies by changing appropriate model inputs seems possible as around 1–9% deviation needs to be explained. However, the second order frequencies show discrepancies of 20–50%. The latter could raise the suspicion that fundamental modelling aspects are not included, or that the second order frequencies are significantly more sensitive towards errors in certain parameters.

The largest part of the difference between the *OWI-lab: Nominal* and *Design: Nominal* can be explained by differences in the foundation stiffness; as mentioned in Section 2.3, the OWI-lab integrated FE model uses re-interpreted CPT data, in combination with the PISA formulation, to derive soil curves. These curves are on average stiffer than the soil curves initially used by the designer and therefore result in higher natural frequencies for the integrated FE model.

The error on the second order frequencies is expected to be rooted in the foundation and hydrodynamic modelling, since the tower and the RNA are identical throughout the farm. However, it should be noted that the measured second order frequencies have been corrected for tidal levels, and that this correction can introduce an additional source of uncertainty.

It should be noted that the results for the designer's stiff scenario (*Design: stiff*) do slightly deviate from the relative frequencies corresponding to the other scenarios. Beside a slightly larger spread, the frequencies show what seems to be an upward trend for the OWT numbers between 35-50. These differences can, to date, only be explained by site specific sensitivities to differences in the modelling assumptions presented in Table 1.

4. Sensitivity assessments

In this section the results of the individual sensitivity studies are presented; an overview of the selected parametrizations had been given in Table 2. In Table 3, an overview of indicative soil groupings and their average L/D is given; these soil groups correlate with the layering of the soil, as well as the the penetration depth, and will be used to color code the resulting sensitivities.

Table 3. Indicative clustering based on soil properties and L/D ratio.

Soil group	SG: 1	SG: 2	SG: 3	SG: 4	SG: 5
L/D	5.86	5.61	6.97	6.01	6.37

4.1. Load case dependent py-linearization

The results in Figure 3 show the farm-wide sensitivity of natural frequencies as function of the (static thrust) load which is assumed for linearizing the p-y curves. The considered load range is chosen such that it contains operational and parked load levels; during operation the static thrust load is in the order of several 100 kN, whereas an effective constant load in parked condition is significantly smaller, if not negligible, and mainly attributed to e.g aerodynamic drag forces.

The sensitivities shown in Figure 3 can roughly can be divided into a low load (1N - 50kN) and high load regime (50kN - 500kN). The low load regime can further be subdivided into the load regime for which the linearized spring stiffness values of the sand layers approach their initial stifness, and the regime for which the stiffness values of the clay layers approach their initial stifness values; these two regimes are visible by a flattening of the sensitivities between 1kN and 30kN, and the sudden increase of the sensitivities between 1N and 0.1kN, respectively.

For the high load regime (50kN - 500kN), an approximately linear downward trend can be observed which shows that increasing the load will result in a softer soil-response, which is to be

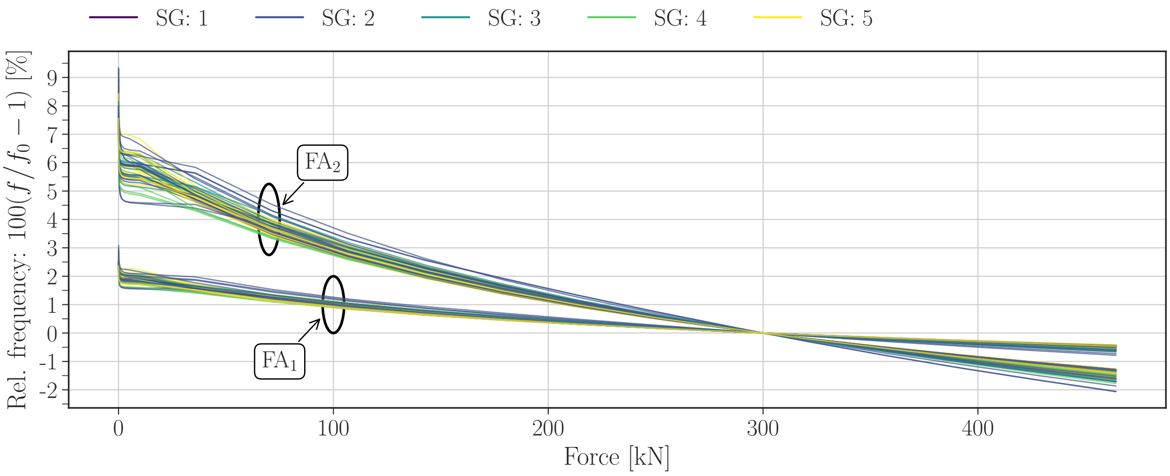

Figure 3. Sensitivity of the first and second order natural frequencies in fore-aft direction with respect to a variation in the thrust load used for the linearization of the p-y curves. See table 3 for soil group information.

expected since the secant modulus of the used p-y curves is decreasing with increasing deflection (load levels). Hence, when increasing the load, the considered natural frequencies will decrease.

For the low load regime (1N - 50kN), decreasing the load below 50kN shows a increasingly non linear change of the natural frequencies. As mentioned, for very lower loads, the linearization of the p-y curves will result in linear spring stiffness coefficients which are increasingly approximating the initial stiffness values of sand and clay; the latter can be observed by a gradual flattening of the the curves as well as steep incline for the lowest load values. The results show a maximum increase of $\approx 3\%$ for the first order natural frequency compared to the reference model, while the second order frequencies increases by up to $\approx 9\%$.

Since an equivalent thrust load during parked conditions is expected to be significantly lower than during nominal operation, it could be argued that the low load regime will result in more representative linear soil spring stiffness values, and that frequencies computed with the stiff modelling scenario are more representative for the measurements conducted during parked conditions (see section 3). Finally, when taking the different soil groups into account it is noticeable that the natural frequencies of the more deeply embedded foundations are, on average, a little less sensitive to changes in the linearization load case compared to the more shallow ones.

4.2. Soil stiffness

The sensitivities of the first and second natural frequencies in fore-aft direction, with respect to a scale factor applied to all soil spring stiffness values, are presented in Figure 4. Whereas it is possible to assess the effects of individual soil layer/types, for this contribution it is chosen to scale the complete stiffness profile in order to assess the upper bound of the sensitivity with respect to the soil spring stiffness values.

Figure 4 shows that increasing the soil stiffness, will also increase the natural frequencies and visa versa. For the first fore-aft frequency, a doubling of the stiffness results in about a 1.5% frequency increase, whereas halving the spring stiffness will result in an average of a 2% frequency decrease; the second fore-aft frequencies are a bit more responsive and gain up to 5% or fall by 6% respectively. When scaled up to the extremes, up to 10 times the original

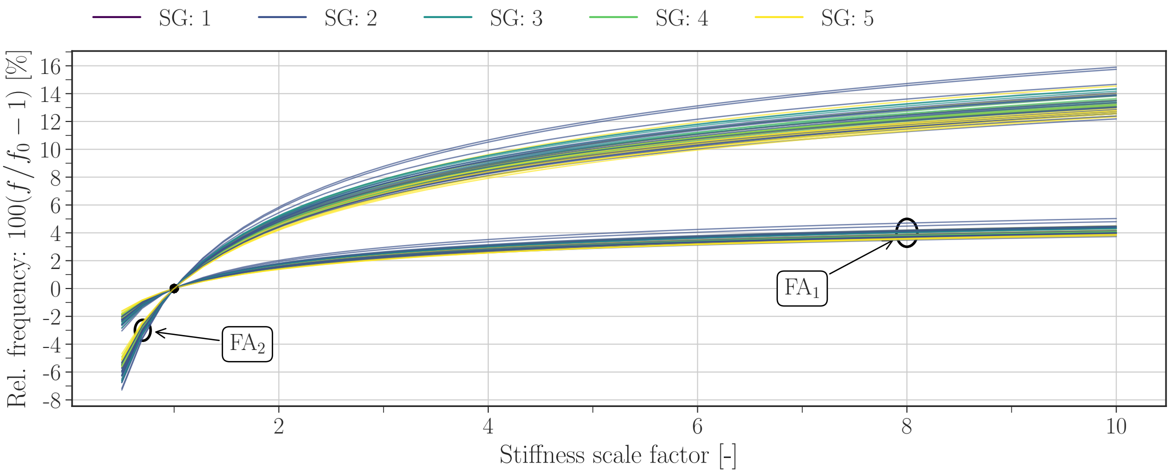

Figure 4. Sensitivity of the first and second order natural frequencies in fore-aft direction with respect to a scaling of the soil spring stiffness values. See table 3 for soil group information.

stiffness, it appears that the first order natural frequency slowly approaches a limit, and has reached an $4-5\%$ increase; the sensitivities of the second fore-aft frequencies however, seem still be in an increasing trajectory, and have reached an increase (12%+). Finally, when taking into account the different soil groups and slenderness it is noticeable that the more deeply embedded foundations have, on average, a little less response compared to the more shallow ones.

The sensitivity of the mode shapes of a single turbine with respect to the considered parametrization are presented in Appendix B.1. These results are left out of the scope of this article since it is not possible to identify mode shapes using the single sensor setup which is used for the design verification studies; hence, the computed mode shapes cannot be compared against identified counterparts.

4.3. Local Scour depth

In this section the sensitivity of the first and second natural frequency in fore-aft direction, with respect to scour, will be presented [21]. The focus in this study will be on the assessment of the local scour phenomenon [13]. The results of the sensitivity assessment are shown in in Figure 5. The depth of the scour pit has been defined as a multiple of the monopile diameter (D). As such, the range of the investigated depths has been set from $0D$ up to $2D$. This interval should contain realistic values, and for the considered soil profiles also make sure that only the upper sand layers are exposed to numerical scour. Although, adding scour will initially not help to explain the discrepancies between the computed and the measured frequencies as it will decrease the stiffness of the overall structure, it may prove useful to fine tune to specific sites and individual OWT's in a later stage.

As expected, introducing scour leads to a more flexible structure, whose first and second fore-aft natural frequency, on average, reduce by respectively $\approx 5\%$ of and $\approx 10\%$ due to a scour pit of depth $1D$. Just as in the previous subsections, soil groups representing the more shallowly embedded OWT's are more sensitive to introducing scour (ST:1). Considering the range of frequency reductions over all turbines, it can be seen that with an increasing scour depth the range increases, showing a significant spread and clearly underlining the site and turbine specific effect of scour. As a final note, the OWI-model has the option to add a scour protection layer on top of the mudline, resulting in a potentially stiffer foundation; However, it was decided to

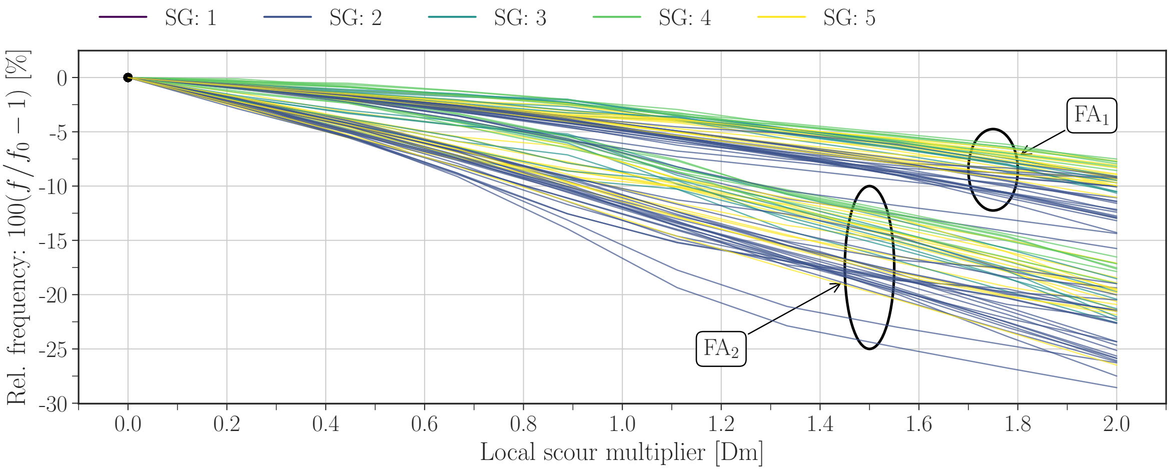

Figure 5. Sensitivity of the first and second order natural frequencies in fore-aft direction with respect to a variation of the local scour depth. See table 3 for soil group information.

leave this feature out of this study since the validity of the used model is still part of ongoing research.

4.4. Rotor nacelle assembly

In this section the sensitivity of the first and second natural frequency in fore-aft direction, with respect to changes in the RNA mass, will be presented; the results of the sensitivity assessment are shown in in Figure 6. Because changes in the rotational inertia terms had a negligible effect on the computed frequencies, only the lumped mass terms have been varied.

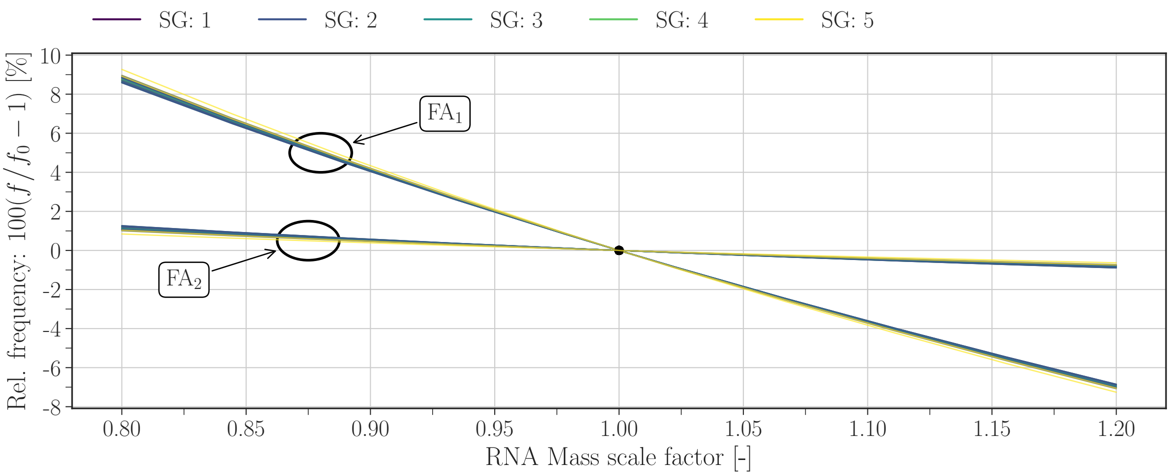

Figure 6. Sensitivity of the first and second order natural frequencies in fore-aft direction with respect to scaling of of the RNA mass. See table 3 for soil group information.

The results show that the RNA mass has a significant effect on the first fore-aft frequency. However it should be noted that the uncertainty on the total mass is relatively low, and that the range over which this study has been conducted does not represent an expected uncertainty bound. Instead these values were only used to test the response of the OWI-lab integrated FE model, and assess what potential effects could be attributed to extreme mass changes.

For the first order natural frequencies there is a clear trend of a 2% frequency change per 5% RNA mass change, where lowering the mass yields higher frequencies and visa versa. The sensitivity of the second fore-aft frequency is a significantly lower, as it only tends to change 0.25% in frequency per 5% RNA mass change. Just like the first order fore-aft frequencies, the computed sensitivities show little spread. The spread of the curves is notably very small, i.e. changing the top mass on farm-wide level does have a very consistent effect on the first and second order natural frequencies. Regarding the modelling of the RNA, it is considered to be a simplified representation which can be improved, in order to reach a more conclusive outcome on the effect of the RNA modelling as well as specific RNA parameters.

The sensitivity of the mode shapes of a single turbine with respect to the considered parametrization are presented in Appendix B.2. These results are left out of the scope of this article since it is not possible to identify mode shapes using the single sensor setup which is used for the design verification studies; hence, the computed mode shapes cannot be compared against identified counterparts.

5. Conclusions

When comparing the measurements with the nominal OWI-lab integrated FE model, a rather large discrepancy is found for both the first $(1.0\% - 7.5\%)$ and second $(25\% - 50\%)$ order natural frequencies. The observed discrepancies can be slightly reduced if the following assumption can be made. "When measuring the natural frequencies of an OWT in parked mode, the initial soil stiffness can be used to model the foundation." In this publication, this translates to using the initial soil stiffness while deriving the stiffness of the linear elastic foundation model of the in-house integrated model. When using this assumption the discrepancies on the first order natural frequencies could potentially be reduced further by adapting a combination of the stiffness of the soil springs as well as the RNA mass parameters. Furthermore, the effect of including a scour protection will contribute to reducing the discrepancies. However, even the combined effect of these measures still leaves a sizeable gap between the measured and computed second order frequencies. As such, it seems that a more targeted approach is needed in order to pinpoint why the modelled second order frequency deviates so much from the measured frequencies. The final observation is the effect of the relative penetration depth on the model sensitivities. For this data set the average L/D value lies between from 5.86 up to 6.37 and, even within this small bandwidth, it was clear that this impacted the computed sensitivities for different parameters. As was mentioned, the full PISA model was not used as there was no tangible difference when comparing with the a more simplified model which only uses the lateral p-y PISA springs. As such, any conclusions one draws from the results of this dataset should only be applied to OWT-farms with the same or even greater embedded foundation slenderness. If the L/D value starts dropping below 5 and gets into the 3-4 range, it is advised to use the complete PISA model and double check if the responses and assumptions of this publication still fully apply.

Acknowledgments

The author, Dominik Fallais, would like to acknowledge the support of the Belgian Ministry of Economic Affairs through the ETF project PhairywinD.

References

[1] Meetnet Vlaamse Banken.
[2] DNV GL AS. Dnvgl-st-0437: Loads and site conditions for wind turbines. *dnv gl*, 2016.

[3] Daniel Thomas Bartilson. Model updating in structural dynamics: advanced parametrization, optimal regularization, and symmetry considerations. page 135.

[4] Stuyts Bruno. OWI-Lab metadatabse api demonstration.

[5] Harvey J. Burd, David M. G. Taborda, Lidija Zdravković, Christelle N. Abadie, Byron W. Byrne, Guy T. Houlsby, Kenneth G. Gavin, David J. P. Igoe, Richard J. Jardine, Christopher M. Martin, Ross A. McAdam, Antonio M. G. Pedro, and David M. Potts. PISA design model for monopiles for offshore wind turbines: application to a marine sand. *Géotechnique*, 70(11):1048–1066, November 2020.

[6] Byron W. Byrne, Guy T. Houlsby, Harvey J. Burd, Kenneth G. Gavin, David J. P. Igoe, Richard J. Jardine, Christopher M. Martin, Ross A. McAdam, David M. Potts, David M. G. Taborda, and Lidija Zdravković. PISA design model for monopiles for offshore wind turbines: application to a stiff glacial clay till. *Géotechnique*, 70(11):1030–1047, November 2020.

[7] Wystan Carswell. "soil-structure modeling and design considerations for offshore wind turbine monopile foundations.". *University of Massachusetts Amherst*, 2015.

[8] Christof Devriendt, Filipe Magalhães, Wout Weijtjens, Álvaro Cunha, Gert De Sitter, and Patrick Guillaume. Automatic identification of the modal parameters of an offshore wind turbine using state of the art operational modal analysis techniques. page 12, Guimarães, May 2013.

[9] Christof Devriendt and Wout Weijtjens. Damping of offshore wind turbines, 2017.

[10] Christof Devriendt, Wout Weijtjens, Mahmoud El-Kafafy, and Gert De Sitter. Monitoring resonant frequencies and damping values of an offshore wind turbine in parked conditions. *IET Renewable Power Generation*, 8(4):433–441, May 2014.

[11] B. Byrne et al. "new design methods for large diameter piles under lateral loading for offshore wind applications,". *Frontiers in Offshore Geotechnics III*, 2015.

[12] A N Iliopoulos, W Weijtjens, D Van Hemelrijck, and C Devriendt. Prediction of dynamic strains on a monopile offshore wind turbine using virtual sensors. *Journal of Physics: Conference Series*, 628:012108, July 2015.

[13] American Petrolium Institute. Geotechnical and Foundation Design Considerations: ISO 19901-4:2003 (Modified), Petroleum and natural gas industriesSpecific requirements for offshore structures, Part 4Geotechnical and foundation design considerations. *American Petrolium Institute*, 2011.

[14] Dan Kallehave, Byron W. Byrne, Christian LeBlanc Thilsted, and Kristian Kousgaard Mikkelsen. Optimization of monopiles for offshore wind turbines. *Philosophical Transactions of the Royal Society A: Mathematical, Physical and Engineering Sciences*, 373(2035):20140100, February 2015.

[15] K. Maes, A. Iliopoulos, Wout Weijtjens, Christof Devriendt, and G. Lombaert. Dynamic strain estimation for fatigue assessment of an offshore monopile wind turbine using filtering and modal expansion algorithms. *Mechanical Systems and Signal Processing*, 76-77:592–611, August 2016.

[16] Luuk Middelweerd. Sensitivity analysis of the first natural frequency of the offshore wind turbines in the Eneco Luchterduinen wind farm. Master's thesis, TU Delft, December 2017.

[17] John E. Mottershead, Michael Link, and Michael I. Friswell. The sensitivity method in finite element model updating: A tutorial. *Mechanical Systems and Signal Processing*, 25(7):2275–2296, October 2011.

[18] Rasoul Shirzadeh. *Dynamic modeling and analysis of a monopile Offshore Wind Turbine focused on damping and new monitoring strategies.* PhD Thesis, Vrije Universiteit Brussel, Brussel, March 2015.

[19] Ellen Simoen, Guido De Roeck, and Geert Lombaert. Dealing with uncertainty in model updating for damage assessment: A review. *Mechanical Systems and Signal Processing*, 56-57:123–149, May 2015.

[20] W.G. Versteijlen, F.W. Renting, P.L.C. van der Valk, J. Bongers, K.N. van Dalen, and A.V. Metrikine. Effective soil-stiffness validation: Shaker excitation of an in-situ monopile foundation. *Soil Dynamics and Earthquake Engineering*, 102:241–262, November 2017.

[21] Richard J.S. Whitehouse, John M. Harris, James Sutherland, and Jon Rees. The nature of scour development and scour protection at offshore windfarm foundations. *Marine Pollution Bulletin*, 62(1):73–88, January 2011.

[22] Minjie Zhu, Frank McKenna, and Michael H. Scott. OpenSeesPy: Python library for the OpenSees finite element framework. *SoftwareX*, 7:6–11, 2018.

Appendix A. Frequency sensitivities

Table A1 presents the sensitivity of the first and second fore-aft natural frequencies as function of selected parameters; the first four parametrizations have been assessed in the results section of this article, whereas the last four have not been discussed in the main text, and are included to give a wider view on potentially relevant parametrizations.

In Table A2, the differences between the tidal correction based on the assessment from measurement data (section 2.1), as well as the tidal correction derived from numerical sea water level variations (Table A1) are presented. As can be seen, these values suggest that the average modelled correction is slightly higher than the correction derived from in-situ measurements. Based on this observation it is expected that the added mass coefficient used in the nominal model could be slightly to high. Lowering the added mass coefficient would mean that upon removing 1m of water, less mass is removed, potentially reducing the tidal correction. However, when looking at the effect of the added mass coefficient as listed in Table A1, it can be seen that the effects on the first and second fore-aft, as well as side-side, modes is small compared to the observed discrepancies between computed and measured frequencies.

Table A1. Sensitivity ranges for parametrizations presented in Section 4 as well as additional parametrizations

Parametrization	Value	1FA	1SS	2FA	2SS
Static thrust load	1 [N]	$+2.48\%^{+0.61}_{-0.48}$	$+2.46\%^{+0.60}_{-0.48}$	$+7.80\%^{+1.55}_{-1.74}$	$+7.56\%^{+1.51}_{-1.64}$
	300 [kN]	–	–	–	–
	500 [kN]	$-0.61\%^{+0.13}_{-0.32}$	$-0.61\%^{+0.13}_{-0.31}$	$-1.77\%^{+0.28}_{-0.67}$	$-1.73\%^{+0.28}_{-0.67}$
soil stiffness	$*0.5$ [−]	$-2.24\%^{+0.50}_{-0.80}$	$-2.22\%^{+0.50}_{-0.80}$	$-5.89\%^{+0.91}_{-1.29}$	$-5.76\%^{+0.94}_{-1.31}$
	$*1$ [−]	–	–	–	–
	$*10$ [−]	$+4.15\%^{+0.87}_{-0.42}$	$+4.12\%^{+0.87}_{-0.42}$	$+13.36\%^{+2.53}_{-1.18}$	$+12.92\%^{+2.46}_{-1.31}$
local scour	$0D$ [m]	–	–	–	–
	$1D$ [m]	$-4.18\%^{+1.77}_{-3.03}$	$-4.15\%^{+1.76}_{-3.01}$	$-10.37\%^{+4.44}_{-6.28}$	$-10.16\%^{+4.32}_{-6.24}$
	$2D$ [m]	$-10.27\%^{+2.76}_{-5.49}$	$-10.20\%^{+2.74}_{-5.46}$	$-21.54\%^{+5.00}_{-7.03}$	$-21.21\%^{+4.88}_{-7.03}$
RNA mass	$*0.8$ [−]	$+8.77\%^{+0.50}_{-0.18}$	$+8.69\%^{+0.47}_{-0.17}$	$+1.14\%^{+0.13}_{-0.29}$	$+0.92\%^{+0.15}_{-0.41}$
	$*1$ [−]	–	–	–	–
	$*1.2$ [−]	$-6.96\%^{+0.11}_{-0.30}$	$-6.91\%^{+0.11}_{-0.28}$	$-0.81\%^{+0.18}_{-0.09}$	$-0.64\%^{+0.28}_{-0.10}$
C_M	1 [−]	$+0.13\%^{+0.04}_{-0.09}$	$+0.13\%^{+0.04}_{-0.09}$	$+2.14\%^{+0.18}_{-0.76}$	$+2.05\%^{+0.20}_{-0.81}$
	1.2 [−]	–	–	–	–
	2 [−]	$-0.52\%^{+0.35}_{-0.16}$	$-0.51\%^{+0.35}_{-0.16}$	$-7.38\%^{+2.28}_{-0.48}$	$-7.16\%^{+2.47}_{-0.53}$
Wall thickness	−1 [mm]	$-1.21\%^{+0.07}_{-0.20}$	$-1.22\%^{+0.07}_{-0.21}$	$-1.31\%^{+0.09}_{-0.31}$	$-1.37\%^{+0.10}_{-0.31}$
	+0 [mm]	–	–	–	–
	+1 [mm]	$+1.15\%^{+0.20}_{-0.07}$	$1.16\%^{+0.20}_{-0.07}$	$1.26\%^{+0.24}_{-0.08}$	$+1.31\%^{+0.29}_{-0.09}$
marine growth	$*0.8$ [−]	$+0.02\%^{+0.01}_{-0.01}$	$+0.02\%^{+0.01}_{-0.01}$	$+0.31\%^{+0.02}_{-0.10}$	$+0.30\%^{+0.02}_{-0.11}$
	$*1$ [−]	–	–	–	–
	$*1.2$ [−]	$-0.02\%^{+0.01}_{-0.01}$	$-0.02\%^{+0.01}_{-0.01}$	$-0.31\%^{+0.10}_{-0.02}$	$-0.30\%^{+0.11}_{-0.24}$
Sea water level	−1 [mLAT]	$+0.35\%^{+0.08}_{-0.20}$	$+0.35\%^{+0.08}_{-0.19}$	$+4.83\%^{+0.26}_{-0.35}$	$+4.66\%^{+0.20}_{-0.61}$
	+2 [mLAT]	–	–	–	–
	+5 [mLAT]	$-0.39\%^{+0.20}_{-0.07}$	$-0.39\%^{+0.20}_{-0.07}$	$-4.24\%^{+0.29}_{-0.28}$	$-4.13\%^{+0.26}_{-0.24}$

Table A2. Comparison of tidal corrections

Tidal correction	f [Hz]	S_{SWL} [%/m]	$f \cdot S_{\text{SWL}}/100$ [Hz/m]
data			0.0205
Lower	1.25	$(4.83 - 0.35)/3$	0.1867
Upper	1.55	$(4.83 + 0.26)/3$	0.2630

Appendix B. Mode shape sensitivities

This section presents the sensitivity of the first and second fore-aft mode shape, for an individual turbine, with respect to two parametrizations. For each considered mode shape, the normalized mode shape amplitudes as well as the difference between the normalized mode shapes at the evaluated parameter values and the nominal normalized mode shapes will be displayed; all mode shapes have been normalized such that their maximum absolute amplitude equals unity. Due to the single sensor setup which is used for the design verification studies it is not possible to derive mode shapes;

Appendix B.1. Soil stiffness

Figure B1 and B2 show the sensitivity of the first and second fore-aft mode shape with respect to a single scale factor applied to the soil spring stiffness values.

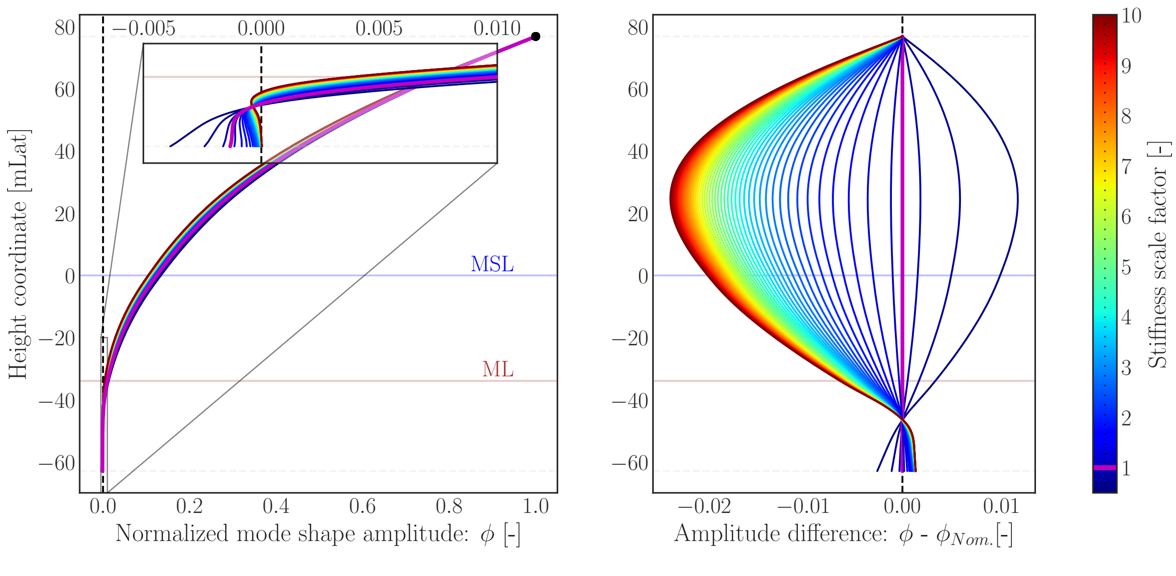

Figure B1. Sensitivity of the first fore-aft mode shape with respect to a scaling of the soil stiffness profile. Left: mode shape amplitudes as function of stiffness scale parameter; right: difference of evaluated modes with respect to mode shape at nominal parameter value.

Looking at the differences between the computed and nominal mode shape reveals that the sensitivity of the second mode is larger compared to the first fore-aft mode. Furthermore it can be observed that scaling the soil stiffness profile will affect the the mode shape over the entire height of the structure, with the largest changes occurring above the mud line level. Considering the first and second fore-aft mode, it can be observed the ratio between the displacement at the mean sea level and the top displacement decreases; this attribute of the shape is of importance for the influence of the wave loading on the structural response. Increasing the stiffness will increase the effectiveness of embedded length, hence a larger part of the embedded length is effective in transferring loads, whereas for lower stiffness values the e.g. top layers might be less effective and therewith reducing the effective embedded length. As a result the point of the maximum bending moment might shift upwards.

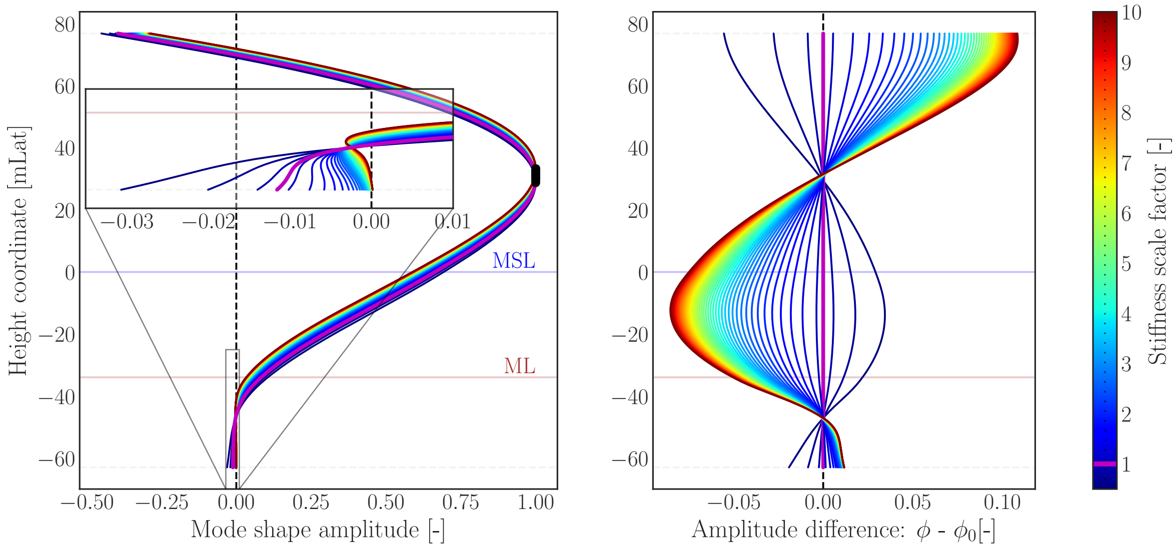

Figure B2. Sensitivity of the second fore-aft mode shape with respect to a scaling of the soil stiffness profile. Left: mode shape amplitudes as function of stiffness scale parameter; right: difference of evaluated modes with respect to mode shape at nominal parameter value.

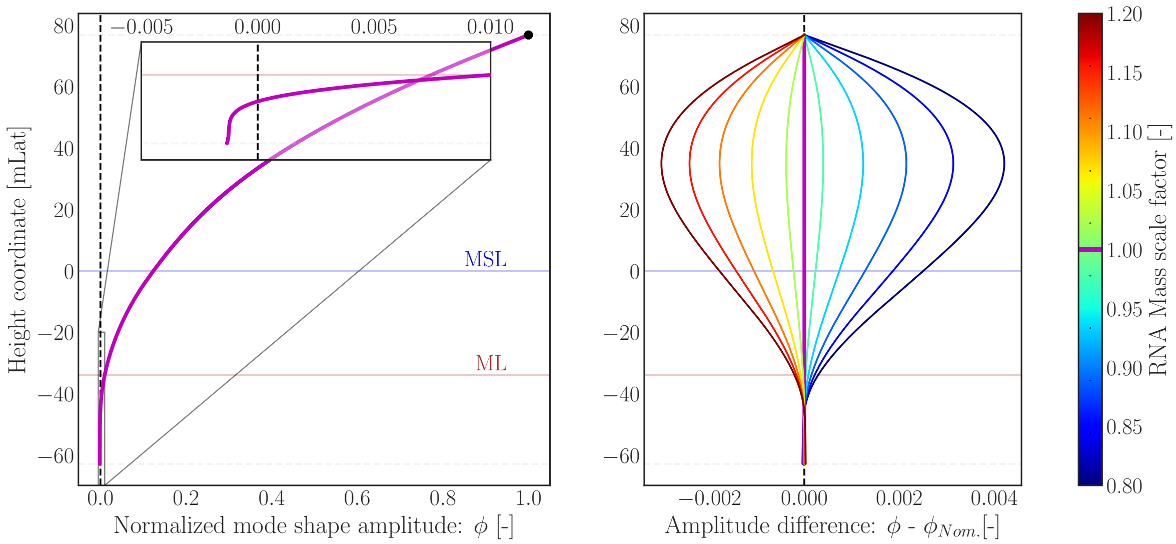

Figure B3. Sensitivity of the first fore-aft mode shape with respect to a scaling of the RNA mass. Left: mode shape amplitudes as function of stiffness scale parameter; right: difference of evaluated modes with respect to mode shape at nominal parameter value.

Appendix B.2. Rotor nacelle assembly

Figure B3 and B4 shows the sensitivity of the first and second fore-aft mode shape with respect to a single scale factor applied on the RNA mass.

For both modes, the effect of the RNA mass can be seen mainly on the wet and dry region of the structure, whereas the shape on the soil domain remains largely unaffected; It should be noted that the effect on the shape of the first fore-aft mode is very small compared to the second mode, as well as the modes presented in the previous section. For the second fore-aft mode the largest effect on the mode shape can be observed for the top part of the structure.

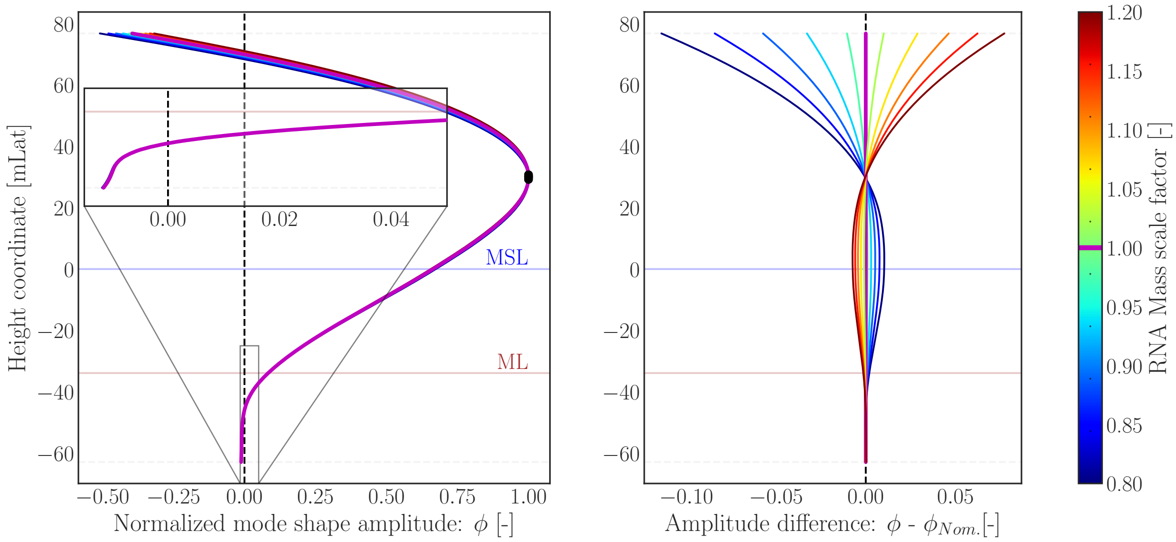

Figure B4. Sensitivity of the second fore-aft mode shape with respect to scaling of the RNA mass. Left: mode shape amplitudes as function of stiffness scale parameter; right: difference of evaluated modes with respect to mode shape at nominal parameter value.